Wavelength modulation spectroscopy using novel mechanical light chopper blade designs

Jayeeta Bhattacharyya, Sandip Ghosh, and B. M. Arora

Articles you may be interested in

Wavelength modulation spectroscopy using novel mechanical light chopper blade designs

Jayeeta Bhattacharyya, Sandip Ghosh,[a) and B. M. Arora
Department of Condensed Matter Physics and Material Science, Tata Institute of Fundamental Research, Homi Bhabha Road, Mumbai 400005, India

We describe two mechanical light chopper blade designs that can be used, with a monochromator and broadband light-source-based spectroscopy setup, to perform wavelength modulation spectroscopy. The left and the right half of a beam emerging from a monochromator would have spectral distributions that are skewed to longer and shorter wavelengths about the central wavelength for positive grating orders. Our two designs, the alternating double-slot blade and the vertical right-angled blade, allow switching between the two halves of the beam front to generate a small periodic variation in the wavelength distribution, enabling wavelength modulation spectroscopy. In contrast to existing methods of wavelength modulation, this technique does not require modification of the monochromator or the light source unit. We analyze the signal waveforms and show how, and under what conditions, wavelength modulation data can be extracted from the alternating signal components measured by the detector. To demonstrate their functioning and applicability, we have performed wavelength-modulated reflectance spectroscopy on epitaxial semiconductor samples using these chopper blades. © *2005 American Institute of Physics.*
[DOI: 10.1063/1.1986970]

I. INTRODUCTION

In modulation spectroscopy one measures a change in the optical response of a sample as a function of wavelength. The change may be due to either an external perturbation such as temperature/electric field or an internal effect arising from a change in the property of the probe beam such as the wavelength or polarization. Wavelength modulation[1,2] is the simplest internal modulation technique where one measures the change in the optical response of a sample due to a small change in the wavelength of the probe beam. For example, in wavelength-modulated reflectance (WMR) spectroscopy, one measures the difference in reflectance of a sample due to a small change in the wavelength around a central wavelength, which is scanned. This results in a spectrum which is the first wavelength derivative of the reflectance spectrum. For crystalline solid samples, this measurement will bring out small changes in the reflectance that occur at photon energies close to the critical-point energies in their electronic band structure. The derivative spectral line shapes give important information about the critical points and hence the electronic band structure. The derivative nature also enables measurement of small changes over large backgrounds. Simplicity in terms of analysis, wide temperature capability, and ability to reveal transitions at energies higher than the band gap makes wavelength modulation very useful for characterization of bulk and heterostructure semiconductors. It can be applied over a wide wavelength range, including wavelength modulation of x-ray absorption fine structure (XAFS) spectra with synchrotron sources.[3]

Typically though, for such measurements one uses a monochromator and broadband lamp source combination, wherein wavelength modulation is achieved by introducing (i) a vibrating mirror/transparent plate in the lamp housing.[4,5] This results in the angle of the beam incident on the monochromator grating to vary periodically by a small amount leading to a periodic variation in the wavelength at the exit slit position. Wavelength modulation is also achieved by introducing (ii) a vibrating mirror just before the exit slit of the monochromator,[6,7] thereby periodically scanning a wavelength-dispersed band of light across the exit slit, or (iii) vibrating the exit slit itself[8,9] so that the slit scans the wavelength-dispersed light band, again resulting in a periodic change in the wavelength of the emergent light about a central wavelength. The difference in the optical response signal is measured by a phase-sensitive detection technique using a lock-in amplifier that locks on to the vibrations of the mirror, plate, or slit, as the case may be. The working principle of the wavelength-modulated XAFS spectroscopy mentioned earlier is equivalent to vibrating the monochromator exit mirror. We note that all the above techniques involve modification of the basic instrument, that is, either the monochromator or the lamp source housing, and this is usually nontrivial.

In this paper we describe two new mechanical chopper blade designs with which one can perform wavelength modulation. The main advantage of this technique is that, since the choppers are placed beyond the monochromator exit slit, it does not require the modification of either the lamp source housing or the monochromator. In the following sections we first describe the working principle and design of the two chopper blades. We analyze the Fourier components

---

a)Electronic mail: sangho10@tifr.res.in
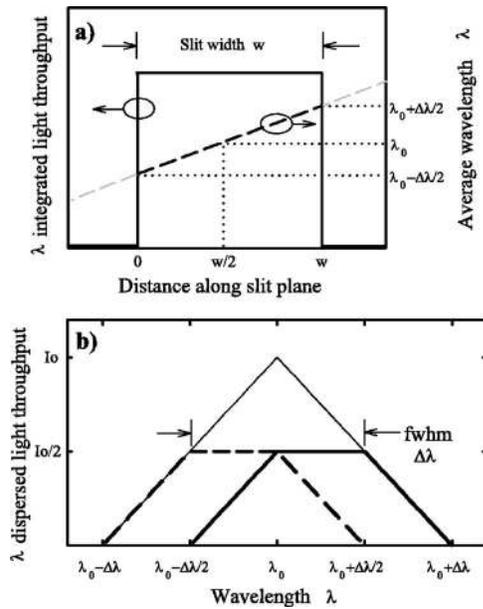
76, 083903-1

FIG. 1. Schematic showing a) variation of the wavelength-integrated intensity and the average wavelength of the light emerging from a monochromator across the exit slit. b) The spectral distribution of the light emerging from the left half (bold dashed line), right half (bold continuous line) and full exit slit (thin continuous line) at the slit plane.

of the signal waveforms generated by these choppers to show how the wavelength modulation signal is to be extracted. We discuss defects in chopping that give rise to unwanted signal components and their minimization by appropriate phase setting on the lock-in amplifier. Thereafter, to demonstrate their applicability, we use them to perform WMR spectroscopy on epitaxially grown semiconductor samples.

II. PRINCIPLE OF OPERATION

The light emerging from a monochromator's exit slit is a convolution of the true lamp spectrum and the instrumental spectral function. The normal dispersion of a grating monochromator[10] results in a monotonic variation in the average wavelength of the light across the exit slit, as depicted in Fig. 1(a). The wavelength-integrated beam profile is rectangular in shape (silt image), while the wavelength-dispersed profile at the slit plane looks triangular (for equal input and output slit width), peaking at the central wavelength λ_0, as shown by the large triangle in Fig. 1(b). At the slit plane, the light emerging from the left (right) half of the exit slit has a trapezoidal wavelength distribution shown by a bold dashed line (bold continuous line). As we move some distance away from the slit plane, the spectral distribution of light in the left half and the right half of the beam front changes, with the center wavelength of each half being closer to λ_0. If we place a mechanical light chopper close to the exit slit of the monochromator, which periodically exposes the left and then the right half of the beam emerging from the exit slit, then the light incident on the sample will periodically differ in wavelength distribution. Assume for now that the spectral response of the measurement system, which includes the lamp, the monochromator grating, the detector, and the optics, is wavelength independent. Then if the response of the sample
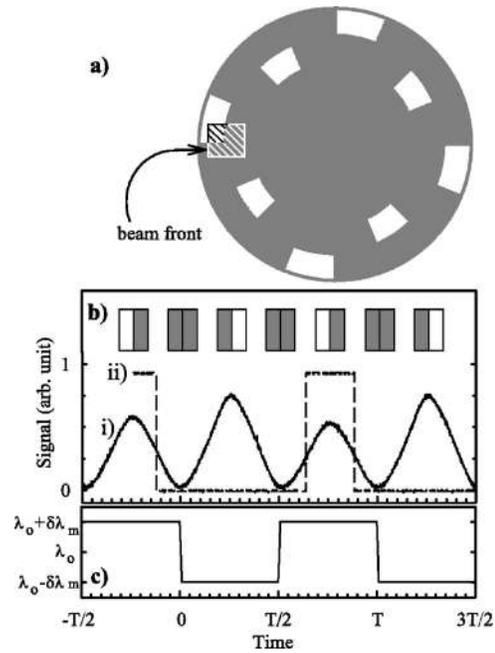

FIG. 2. a) Schematic of the ADS chopper blade and b) (i) actual recorded signal (continuous line) from the detector in a WMR measurement (T = 5.7 ms). The blocking and unblocking of the two halves of the beam front, which results in this signal pattern, is shown schematically. (ii) The signal derived from the optocoupler (dashed line) for providing reference to the lock-in amplifier. c) Schematic of the time dependence of the average wavelength of light emerging through the ADS blade.

differs for these two wavelength distributions, one can measure the wavelength modulation signal from the periodically varying signal generated in the detector using phase-sensitive detection techniques.

Our approach to achieving wavelength modulation has the following drawback. In a typical measurement setup the monochromator's exit slit is imaged on to the sample, and therefore if the sample is inhomogeneous on the scale of the slit image ($\sim$0.25 mm^2), then the difference signal will have an undesirable component arising from this inhomogeneity. However, for inhomogeneities of a much smaller scale, as is typical in epitaxial growth of semiconductors with wafer rotation facility, this is not a problem. Our approach also differs from the vibrating mirror/slit/plate modulation mechanisms in that while in the latter case the overall throughput of light does not change as the wavelength is modulated, in our case the throughput is also modulated. This therefore requires a careful analysis of the time-varying signal measured by the detector in order to obtain the wavelength modulation signal. In the following sections we describe in detail our two chopper blade designs that enable periodic switching on and off of the two halves of the beam front emerging from a monochromator and the analysis of the signal from the detector.

A. Alternating double-slot chopper blade

The alternating double-slot (ADS) blade design has two sets of radially displaced, even number of slots close to the edge of a circular blade, as shown in Fig. 2(a). The outer and inner slots have an equal angular spread and are displaced by a slotless region, which is also of the same angular spread.

This chopper is placed just after the exit slit of the monochromator such that the vertical center of the beam emerging from the monochromator is at the same height as the center of this blade. The horizontal center of the beam coincides with the inner (outer) edge of the outer (inner) slots. Then, as this chopper blade rotates, it will alternately expose the left and the right half of the beam periodically. Note that this chopper blade design is different from the usual radially displaced multiple-slot blades provided by several manufacturers. There each pattern has a different number of slots that give rise to different chopping frequencies for the same motor rotation speed. Here both the inner and the outer slots result in the same chopping frequency $f = 1/T$ (detected by an optocoupler through which the outer slots move) but are out of phase by π radian.

Let us consider a WMR measurement. When the light emerging after the ADS chopper is reflected off the sample under study and is detected by a photodetector, the recorded time-varying signal from the detector has the form shown in Fig. 2(b), plot (i). Also shown in Fig. 2(b), plot (ii) is the signal from the optocoupler, which is used as a reference for phase-sensitive detection. For simplicity of analysis we assume the beam front height, when it hits the blade, is the same as the average length of the slots and also that the blade slices the beam front in two equal halves. Then if the system response is I and the sample's reflectance is R, the signal from the detector can be approximated by a triangular waveform with an amplitude proportional to the throughput IR. Its Fourier series representation is given by

$$S(t) = \frac{IR}{2} + \sum_{n=2,6,10\ldots}^{\infty} \frac{4IR}{\pi^2 n^2}\left(2\cos\frac{n\pi}{2} - \cos n\pi \right.$$
$$\left. - 1\right)\cos 2\pi n f t. \tag{1}$$

While the throughput gets modulated, the average wavelength too varies as a rectangular wave, and is shown schematically in Fig. 2(c). Its Fourier series representation is

$$\lambda = \lambda_0 + \frac{8\delta\lambda_m}{2\pi}\sum_{n=1,3,5,\ldots}^{\infty}\frac{1}{n}\sin 2\pi n f t, \tag{2}$$

where $\delta\lambda_m$ is the amplitude of wavelength modulation. Since I and R are both wavelength dependent, we can expand them in a Taylor series around the central wavelength λ_0 as

$$I(\lambda) = I_0 + \delta\lambda I' + \frac{1}{2}(\delta\lambda)^2 I'' \ldots ,$$
$$\tag{3}$$
$$R(\lambda) = R_0 + \delta\lambda R' + \frac{1}{2}(\delta\lambda)^2 R'' \ldots ,$$

where I_0 and R_0 are the values of the system response and sample reflectance at λ_0, I' and R' are their respective first derivatives with respect to wavelength at λ_0 and so on, and $\delta\lambda = \lambda - \lambda_0$. Using Eq. (2) and (3) in Eq. (1) and keeping the dominant terms to order $\delta\lambda$, we get the dc and the first harmonic ac component as

$$\mathrm{dc} = 0.5 I_0 R_0, \quad \mathrm{ac} \approx 0.3\delta\lambda_m (R' I_0 + I' R_0)\sin 2\pi f t. \tag{4}$$

Note that Eq. (1) did not explicitly have a component at f, it arises from the derivative term $(R'I_0 + I'R_0)$, that is, from the finite wavelength dependence of the system response and the sample's reflectivity. This results in the observed difference in the amplitude of two adjacent triangles of the waveform in Fig. 2(b), plot (i). The rest of the analysis is similar to the conventional vibrating slit/mirror/plate methods. The error introduced due to neglecting the higher-order terms in $\delta\lambda$ is usually not significant.[1,6] The amplitude of the ac component at f and the dc component can be measured with a lock-in amplifier and digital voltmeter, respectively. If the system response is wavelength independent, or varies slowly with wavelength compared to the sample's derivative spectral feature, then $I'R$ can be neglected and we get the normalized WMR signal as the ratio

$$\frac{\mathrm{ac}_{\mathrm{ampl}}}{\mathrm{dc}} \approx \frac{1}{R}\frac{dR}{d\lambda}\bigg|_{\lambda_0}\delta\lambda_m \sim \frac{\Delta R}{R}. \tag{5}$$

The approximation involving the wavelength independence of the system response is invoked in all forms of wavelength modulation spectroscopy and suggestions have been made on how to minimize its influence.[1,11] The effective modulation amplitude $\delta\lambda_m$ is of the order of half the bandpass $\sim\Delta\lambda/2$.

In the above analysis, we took for granted that the ADS blade exposes equal halves of the beam front periodically. The resulting expansion in Eq. (1) had no first harmonic term. However, distortion of the waveforms will occur because of unequal beam front division arising from improper placement of the blade, the shape of the beam front, the shape of the slots, and other defects in the chopper blade. Any defect that occurs once in every time interval T, that is, in every open-slot/closed-slot pair, will show up as a first harmonic (f) component in Eq. (1). If the defect is in one out of the m open-slot/closed-slot pairs, then it would give a spurious signal at f, although its magnitude will be reduced because it would be its mth harmonic at f. In general, the asymmetry in the waveform results in the appearance of a first harmonic term, Eq. (1). This would lead to an error component in the first harmonic signal proportional to I_0R_0. This unwanted signal can be minimized by getting the chopper to expose equal halves of the beam front, and a procedure for doing so will be discussed in Sec. III. Thus, in general, the signal from the detector is not simply proportional to the required derivative, and additional steps are required to extract the derivative signal as follows. The first harmonic signal from the detector $S_1(t)$ can in general be expressed as

$$S_1(t) = \alpha\sin(2\pi f t) + \beta\sin(2\pi f t - \phi), \tag{6}$$

where α is the required component that is proportional to the derivative signal and β is the unwanted error component. If the phase on the lock-in amplifier is 0° relative to the pure derivative signal, then the signal in the in-phase channel will have a contribution from both components, as depicted in Fig. 3. However, if the phase is set to an angle ϕ relative to the pure derivative signal, then we will measure an uncontaminated derivative signal in the out-of-phase channel of the lock-in amplifier, although it will be reduced in magnitude.
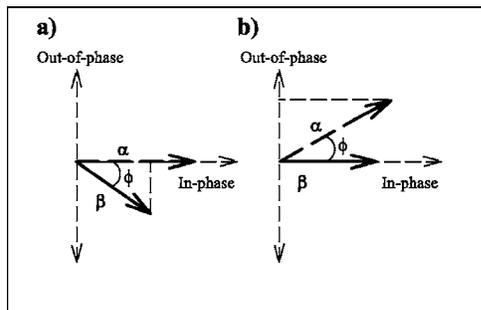
FIG. 3. Phasor diagram showing the in-phase and the out-of-phase components of the signal when the phase on the lock-in amplifier is set to a) 0 and b) angle ϕ relative to the wavelength derivative signal. The WMR signal and the error signal magnitudes are proportional to α and β, respectively.

The angle ϕ needs to be set once for a particular measurement setup and the procedure will be outlined in Sec. (3).

B. Vertical right-angled chopper blade

The vertical right-angled (VRA) blade design consists of a right-angled section fixed at the center of a disk that rotates in the horizontal plane, as shown in Fig. 4(a). A notch on the disk, which passes through an optocoupler, is used to generate the reference frequency for phase-sensitive detection. This chopper is placed just after the exit slit of the monochromator such that the axis of rotation coincides with the center of the beam front emerging from the monochromator. The width of the light beam when it hits the chopper must be $\leq \sqrt{2}L$, where L is the length of one arm of the right-angled blade. This ensures that one half of the beam front remains blocked as long as portions of the other half are allowed to
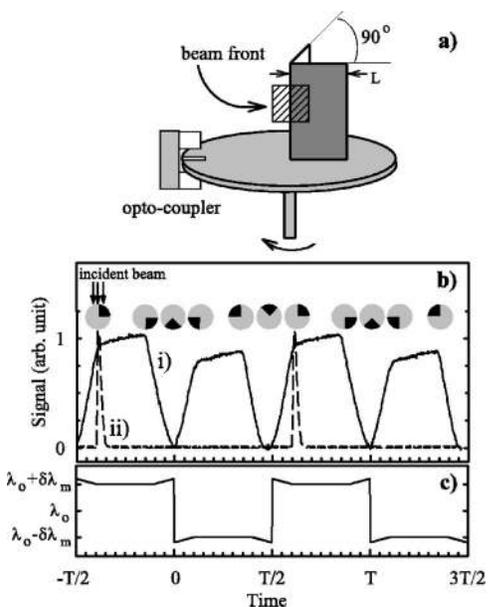

FIG. 4. a) Schematic of the VRA chopper blade and b) (i) actual recorded signal from the detector (continuous line) in a WMR measurement (T =0.04 s). The blocking and unblocking of the two halves of the beam front by the VRA blade as seen from the top, which results in this signal pattern, is shown schematically. (ii) The signal from the optocoupler (dashed line) for providing reference to the lock-in amplifier. c) Schematic of the time dependence of the average wavelength of light emerging through the VRA blade.

pass through. Then as the disk rotates, the right-angled blade exposes the left and the right half of the beam periodically. To analyze its workings we again consider a WMR measurement. When the light emerging after the chopper is reflected off the sample under study and detected by a photodetector, the recorded time-varying signal from the photodetector has a form shown in Fig. 4(b), plot (i). The signal derived from the optocoupler, which is fed as reference to the lock-in amplifier, is shown in Fig. 4(b), plot (ii). The signal in Fig. 4(b), plot (i) can be approximated by a trapezoidal wave. The Fourier series representation of this signal waveform is given by

$$S(t) = \frac{3IR}{4} + \sum_{n=2,4,6,10,12\ldots}^{\infty} \frac{8IR}{\pi^2 n^2}\left(\cos\frac{n\pi}{4} + \cos\frac{3n\pi}{4}\right.$$
$$\left. - \cos n\pi - 1\right)\cos 2n\pi ft. \tag{7}$$

The terms in the above series survive for even n, which are not multiples of 8. Here too the average wavelength varies as a near rectangular wave, as shown schematically in Fig. 4(c). Proceeding with the analysis as in the case of the ADS chopper blade, we get a first harmonic signal having a component proportional to the wavelength derivative and an error component. Then locking on to the first harmonic and with an appropriate phase setting on the lock-in amplifier, we will again measure a signal proportional to just the wavelength derivative in the out-of-phase channel. Then the ratio of this measured first harmonic ac signal amplitude to the dc signal gives the normalized WMR signal. The approximations used here and their range of validity are the same as in case of the ADS chopper. The difference between the ADS and the VRA blades, apart from the slightly more involved construction of the latter, has to do with the sensitivity to errors in blade construction. For the VRA blade, any defect in the blade will have a large first harmonic component at the measurement frequency f, so it is more sensitive to defects in the blade construction. Both the ADS and the VRA blades can be operated with standard chopper controllers.

III. APPLICATION TO WAVELENGTH-MODULATED REFLECTANCE SPECTROSCOPY

For wavelength-modulated measurements using the ADS and VRA chopper blades, the chopper unit has to be mounted on a x-y-z micropositioner and placed such that the blades are as close to the exit slit of the monochromator as possible. One must first choose a sample that has a flat spectral response region that coincides with some flat spectral response region of the system. The system refers to the combination of light source, monochromator, optics, and detector. For this sample, at a wavelength in this flat spectral region, the quantity $(R'I_0 + I'R_0)$ is zero. However, one may still detect a large first harmonic ac signal because the chopper may not be slicing the beam front into two equal halves. One then has to gradually move the chopper across the beam front such that the signal in the lock-in amplifier is minimized. Once minimum signal is achieved, the phase should be set on the lock-in amplifier such that the entire signal is in the X (in-
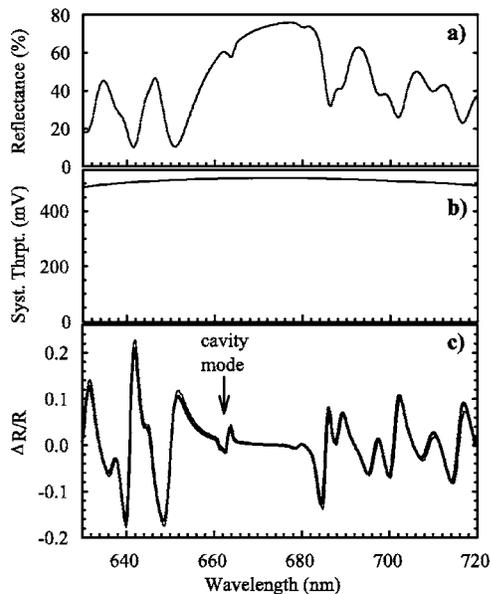
FIG. 5. a) Reflectance spectrum of the VCSEL sample. b) Spectral response of the measurement system's throughput. c) Comparison of the measured WMR spectrum of the VCSEL with an ADS blade (thick line) with the spectrum numerically calculated (thin line) from the reflectance spectrum.
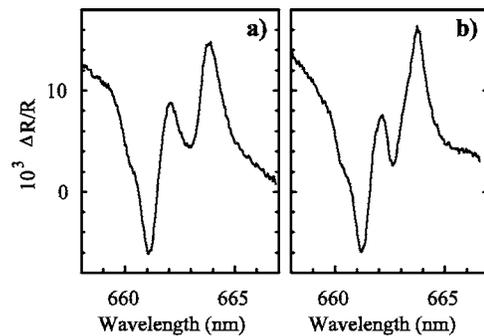

FIG. 6. a) A detail of the measured wavelength-modulated reflectance spectrum, on a different part of the VCSEL wafer, using a VRA blade. b) The numerically calculated spectrum.

phase) channel. This is the error signal that arises due to defects in the chopping that was discussed previously, and the phase setting corresponds to angle ϕ of Fig. 3. After this initial adjustment is done, one can proceed with a wavelength modulation measurement, whose signal will now arise in the Y (out-of-phase) channel of the lock-in amplifier.

To demonstrate the workings of these chopper blades we have performed wavelength-modulated reflectance measurements on epitaxial semiconductor samples grown by the metalorganic vapor phase epitaxy technique. Figure 5(a) shows the reflectance spectrum of an as-grown vertical cavity surface emitting laser (VCSEL) structure. The structure design consisted of two distributed Bragg reflectors (DBR) made of 35 (50) pairs of $AlAs/Al_{0.6}Ga_{0.4}As$ as the top (bottom) reflector sandwiching a lambda-cavity layer of $(Al_{0.7}Ga_{0.3})_{0.5}In_{0.5}P$, with three 6-nm-thick $Ga_{0.44}In_{0.56}P$ quantum wells.[12] The sharp features in its reflectance spectrum is characteristic of the DBRs and the single cavity mode. This sample's growth did not match the design, resulting in a misaligned cavity mode. However, the sharp features in its reflectance spectrum, which are characteristic of the DBRs, is expected to give rise to large signals in a WMR measurement and enable us to verify the workings of our chopper blade designs. From the reflectance spectrum alone it is not immediately clear as to whether the feature at 664 nm or the one at 680 nm represents the cavity mode. Figure 5(b) depicts the spectral response of the measurement setup, which includes the lamp, grating, optics, and detector. It shows a far more gradual change with wavelength when compared to the reflectance spectrum of the VCSEL, so that the approximation in neglecting the $I'R_0$ term is valid. Note that the system response is flat (wavelength independent) at ~667 nm, as is the reflectance spectrum of the VCSEL sample. We used this sample, with the monochromator set at 667 nm, to set the angle ϕ on the lock-in amplifier. Figure

5(c) shows the measured WMR spectrum (thick line) of the VCSEL sample using an ADS blade. In our setup we had a 0.5 m focal length imaging monochromator with a linear dispersion of 1.5 nm/mm, a slit width of 0.5 mm, and the chopper placed at 4 cm from the exit slit. Here $\Delta\lambda \sim 0.8$ nm, so that $\delta\lambda_{mod}/\lambda \sim 6 \times 10^{-4}$ in the spectral range of Fig. 5(a). Also shown in Fig. 5(c) is the numerically calculated and scaled WMR spectrum (thin line) using the reflectance spectrum shown in Fig. 5(a). Evidently the spectral features in the calculated and the measured spectrum match satisfactorily. Note that the cavity mode feature is more clearly brought out in the WMR spectrum when compared to the conventional reflectance spectrum. Measurement with a VRA blade on this sample yielded an identical spectrum. Figure 6(a) shows a detail of the cavity mode region of the spectrum, measured on another part of the VCSEL wafer with a VRA blade. It compares well with the numerically calculated spectrum obtained using a higher-resolution reflectance measurement shown in Fig. 6(b). The comparison also indicates that there is no apparent difference in the noise characteristics between our direct WMR measurement and the numerical derivative of a well-averaged, higher-resolution, normal measurement. Our WMR noise levels may be higher than in the conventional vibrating slit/mirror/plate methods because we have a large ac signal at $2f$ (throughput modulation) that the lock-in amplifier is trying to suppress. However, our approach is still quite useful for real-time measurements, for example, in modulated absorption monitoring of pollutant gases,[13] where one may not have the convenience of averaging and storing the data first over narrowly spaced wavelength intervals with a high resolution and then calculating the derivatives.

Finally we present a WMR measurement at low temperature with an ADS blade. The sample is a $Al_{0.3}Ga_{0.7}As/GaAs$ single quantum well with a well width $L_w \sim 85$ Å. Figure 7(a) shows its WMR spectrum (thick line) at 8 K, revealing two prominent transitions. The transition wavelengths were obtained by fitting Aspnes' line-shape functional form[14] (dashed line). The fit is evidently quite satisfactory and gives transition wavelength values of 791.0 and 797.3 nm, in fair agreement with the theoretical estimate for the ground-state light-hole (788 nm) and heavy-hole (797 nm) exciton transitions of the quantum well, with 10 meV exciton binding energy. Photoluminescence spec-
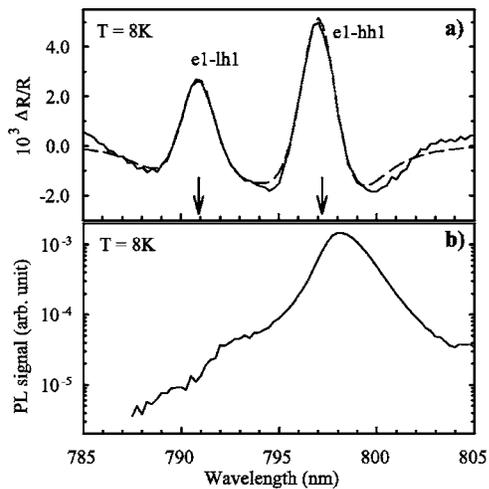
FIG. 7. a) Measured wavelength-modulated reflectance spectrum (continuous line) of an $Al_{0.3}Ga_{0.7}As/GaAs$ quantum well sample ($L_w \sim 85$ Å), using the ADS blade, showing the ground-state heavy-hole and light-hole exciton transitions. The dashed line is the fitted line-shape function. b) The photoluminescence spectrum of this sample.

In principle, such a technique can also be adopted for energy-derivative XAFS with synchrotron sources since there too one has an x-ray beam with wavelengths varying regularly across the beam cross section.

ACKNOWLEDGMENTS

troscopy is usually the most common postgrowth, nondestructive optical characterization tool used to test such structures. Figure 7(b) shows the measured photoluminescence spectrum of this sample where, due to the difference in the occupation probabilities of photogenerated carriers, only the heavy-hole exciton feature is seen, with only a small hint of the light-hole exciton transition. This clearly brings out the usefulness of our chopper blades for wavelength-modulated reflectance measurement in regular semiconductor samples.

[1] M. Cardona, in *Solid State Physics Supplement 11*, edited by F. Seitz, D. Turnbull, and H. Ehrenreich (Academic, New York, 1969).
[2] B. Batz, in *Semiconductors and Semimetals*, edited by R. Willardson and A. C. Beer (Academic, New York, 1972), Vol. 9.
[3] M. Suzuki, N. Kawamura, and T. Ishikawa, Nucl. Instrum. Methods Phys. Res. A **467–468**, 1568 (2001).
[4] L. Lassabatere, C. Alibert, J. Bonnet, and L. Soonckindt, J. Phys. E **9**, 773 (1976).
[5] K. L. Shaklee, J. E. Rowe, and M. Cardona, Phys. Rev. **174**, 828 (1968).
[6] M. Welkowsky and R. Braunnstein, Rev. Sci. Instrum. **43**, 399 (1972).
[7] M. J. Holcomb and W. A. Little, Rev. Sci. Instrum. **63**, 5570 (1992).
[8] I. Balslev, Phys. Rev. **143**, 636 (1966).
[9] J. S. Liang, S. D. Wang, Y. S. Huanga, L. Malikova, F. H. Pollak, J. P. Debray, R. Hoffman, A. Amtout, and R. A. Stall, J. Appl. Phys. **93**, 1874 (2003).
[10] F. A. Jenkins and H. E. White, *Fundamentals of Optics* (McGraw-Hill, New York, 1981).
[11] S. M. Eetemadi and R. Braunnstein, J. Appl. Phys. **58**, 3856 (1985).
[12] A. Bhattacharya, M. Zorn, A. Oster, M. Nasarek, H. Wenzel, J. Sebastian, M. Weyers, and G. Trankle, J. Cryst. Growth **221**, 663 (2000).
[13] T. Izumi and K. Nakamura, J. Phys. E **14**, 105 (1981).
[14] S. Ghosh and H. T. Grahn, J. Appl. Phys. **90**, 500 (2001).